Z. Phys. Chem. **221** (2007) 1287–1305 / **DOI** 10.1524/zpch.2007.221.9–10.1287
© by Oldenbourg Wissenschaftsverlag, München

Monte Carlo Simulation of Kinetically Limited Electrodeposition on a Surface with Metal Seed Clusters

By Timothy O. Drews, Richard D. Braatz, and Richard C. Alkire*

Department of Chemical and Biomolecular Engineering, University of Illinois at Urbana-Champaign, Urbana, IL 61801, USA

Dedicated to Prof. Dr. Dieter M. Kolb on the occasion of his 65th birthday

(Received July 20, 2007; accepted July 23, 2007)

Metal Cluster / Nucleation / Kinetic Monte Carlo / Simulation / Electrodeposition

Kinetic Monte Carlo (KMC) simulations were carried out to simulate kinetic-limited electrodeposition of a metal (M) onto an array of pre-existing metal clusters on a substrate (S) of a second conducting material. Electrochemical reaction and surface diffusion were accounted for in a KMC code which tracked deposit growth with a $(2+1)$-dimensional approach. Beginning with various arrangements of ten-atom metal seed clusters on a substrate platform of 300×300 fcc lattice sites, KMC simulations were carried out to investigate the evolution of the surface morphology. The influence of the number (spacing) of pre-existing seed clusters, the applied potential, and the metal–substrate surface diffusion energy barrier were investigated. It was found that when 16 or fewer seed clusters were present on the surface prior to electrodeposition, the resulting nucleation distribution was dominated by secondary nuclei formed during deposition. For substrates with a metal–substrate surface diffusion energy barrier greater than 3.5×10^{-20} J, it was more difficult to control the uniform growth of the seed clusters owing to the nucleation of secondary clusters. At lower applied potentials it was found that larger nuclei could be grown with a more controlled size distribution because fewer secondary nuclei were formed. Furthermore, it was found that larger clusters with a more controlled size distribution can be grown when more clusters are seeded onto the surface because the deposited atoms were more likely to attach to existing clusters, than to form secondary nuclei.

1. Introduction

Electrochemical deposition of metal in small-scale patterns is used in numerous processes for fabricating novel structures as well as inventive design

* Corresponding author. E-mail: r-alkire@uiuc.edu

concepts for their application. However, the detailed engineering and manufacturability of such devices requires precise quantitative understanding of small-scale phenomena that affect quality control of each step of the processes used in the assembly of such systems. Therefore, interest arises in applying atomistic methods to simulate surface reactions and transport phenomena in electrochemical systems. Such simulations provide insights into small-scale stochastic phenomena, and they provide a capability that augments traditional electrochemical engineering design methods which are based on continuum methods [1, 2]. The present work describes an approach that employs a kinetic Monte Carlo (KMC) method for simulating growth of small metal clusters on the surface of a second conducting material by electrodeposition in a pristine system.

The range of specific systems formed by manipulation of electrochemical surface phenomena is large and growing rapidly, based in large part on a suite of new experimental tools [3–5]. Electrodeposition has been utilized to form novel structures including insertion of specific ions into specified molecular sites [6], atomic layer epitaxy [7], as well as electrochemical fabrication of nanowires [8, 9], nanocubes [10], superlattices[11] and atomically layered nanostructures [12], and materials having unique optical [13, 14], magnetic [15], and catalytic[16] properties. Potential applications for small metal clusters have also been suggested including quantum logic circuits [17], optoelectronics, information storage, and sensing [18].

Several methods have been used to create small metal clusters on substrates. Kolb *et al.*, have used a STM tip to deposit Cu clusters on Au(111) [19]]and Cu clusters on Ag(111) [20]. They have shown that this technique can produce reproducible structures rapidly, in order to form large arrays of nanoclusters [21, 22]. Wiesbeck *et al.* [23], *and* Schindler *et al.* [17] have also developed methods for depositing metal nanodots with a STM. Sander and Tan [18] have used anodic alumina films as templates to deposit nanoparticle arrays. Moore *et al.*, have used patterned substrates to create uniform nanodot arrays of vapor deposited Ti, Cr, and V that can be used in biological sample preparation [24].

The growth of small metal clusters must be controlled to uniform size and spatial distribution if they are to be used in functional devices [25]. For such applications it would be clearly important to avoid formation of secondary nuclei that form spontaneously and would not be a part of the desired structure. Penner and co-workers have shown that electrodeposition of metal particles under kinetic-limited conditions is preferable to growth under diffusion-limited conditions because diffusion limitations lead to a broadening of the cluster size distribution owing to competition for metal ions from the local solution near the particles [26]. They have also shown that particles grown under kinetically limited conditions allow uniform particles to be grown that are 11 times larger than those that can be uniformly grown under diffusion-controlled conditions [26]. Low-overpotential growth of nanoparticles can result in a variance

in particle size that is typically less than 7% [27]. In addition, kinetically limited conditions are important in many electrodeposition systems that involve additives for the control of surface phenomena.

Metal clusters are of technological interest because they exhibit behavior that is different from that of individual atoms as well as the bulk metal, and the relevant theoretical foundations have been recently reviewed [28, 29]. Understanding how to manipulate and control the growth processes that occur during the formation of metal clusters is important, since their functioning in a Nanodevice is dependent on their size [30]. Numerical methods have been developed to simulate the formation of nanoclusters for a system where Co is evaporated onto Au(788), for which the simulation model integrates molecular dynamics and KMC methods [31]. Brown and co-workers combined dynamic Monte Carlo simulations and a lattice-gas Hamiltonian to create a stochastic dynamic model used to investigate the underpotential deposition of Cu with sulfate on Au(111) [32].

Kinetic Monte Carlo simulation methods have been used with success in the analysis of nucleation and growth processes in a variety of physical systems [33, 34]. Various types of KMC models have been used to simulate nucleation onto patterned substrates [35], as well as self-organized island growth [36] in non-electrochemical systems. Del Pópolo and co-workers used grand canonical Monte Carlo simulations to investigate the stability of clusters deposited by Kolb's STM for a variety of metal substrate compositions [37]. Giménez and co-workers used KMC to simulate the nucleation and growth of Ag on Au(111) and Au(100) [38]. Alkire and coworkers have recently reported KMC methods for investigating kinetically limited electrodeposition on a (111) plan of a face-centered cubic lattice on a featureless surface [39] as well as a surface containing monatomic step edges [40].

In the present work, a kinetic Monte Carlo (KMC) simulation model has been developed to simulate the pristine case of kinetically limited electrodeposition onto an array of small pre-existing metal clusters on a substrate of a second metal. The surface processes that were considered include adsorption and electrochemical reaction accompanied by surface diffusion on (111) oriented facets. The effect of operating parameters on a distribution of cluster sizes, including secondary nuclei, was explored. The KMC code has been written so that it may be extended in the future to address additional phenomena associated with solution additives.

2. Simulation model and numerical procedures

The simulation model represents an idealized system in order to focus on nucleation and growth phenomena during electrodeposition of a metal (M) onto a substrate (S) which contains pre-existing seed clusters of metal M. The geometric details of the substrate and deposited metal were purposely kept simple,

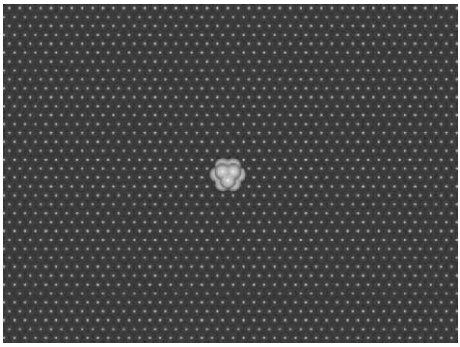

Fig. 1. Initial simulation domain in the vicinity of a single seed cluster having 10 metal atoms on a FCC lattice. The cluster consists of two layers: a hexagonal grouping of seven atoms, with a second layer of three atoms positioned in the three-fold hollow sites.

as was the reaction chemistry. The objective is to simulate a range of deposit morphologies that arise for various combinations of the reaction, transport and geometric parameters. The simulation model and numerical procedures used here follow closely those reported recently in investigation of nucleation and growth in the absence of pre-existing metal seed clusters [39]. Additional details are also available elsewhere [41].

The initial configuration of the simulated surface was an atomically flat (111) facet of an fcc substrate metal (S) consisting of a 300×300 lattice which was decorated with various arrangements of small clusters of deposit metal (M) consisting of ten atoms arranged in two layers as illustrated in Fig. 1. The atomic spacing for the deposited metal and substrate were assumed to be identical; *i.e.*, atoms deposited on the surface are placed at sites that represent an extension of the fcc substrate with the same spacing. Metal ions (M^{2+}) were reduced on either the substrate material (S) or on the metal (M) present on the surface, which could be either in the form of pre-existing seed clusters or M atoms deposited earlier during the simulation. Other than the presence of pre-existing seed clusters, the model and numerical procedures are the same as reported previously [39].

The electrodeposition reaction consists of a one-step reduction of divalent metal ions (M^{n+}) to form metal atoms (M) which may move by surface diffusion to the site of lattice incorporation

$$M^{2+}_{(aq)} + 2e^- \rightarrow M_{(ad)} \tag{1}$$

$$M_{(ad),site\ 1} \rightarrow M_{(ad),site\ 2}\,. \tag{2}$$

No other reactions were considered to occur. Simulations were performed with the assumption of kinetic control under rapid mass transfer conditions, for which the surface concentration of M^{n+} was equal to the bulk value which was

held constant during the course of a simulation. The equilibrium potential for deposition onto metal surface (M) was assigned the reference value of zero; the nucleation overpotential for deposition of metal (M) on substrate surface (S) was assigned a value of -0.100 V, a value typically observed in experiments [42]. The charge-transfer process followed the Butler–Volmer equation on surface M, while recognizing that there was no anodic reactant on the substrate (S). The substrate atoms (S) were assumed not to move. Metal atoms (M) on the substrate were permitted to move by surface diffusion over substrate atoms, as well as over previously deposited metal atoms, until such time that they were covered by another deposited atom. In a single KMC step, metal atoms (M) were restricted in making moves either to a nearest neighbor site in the same plane, or up or down one height level.

The kinetic Monte Carlo (KMC) simulation approach used in this study has been used previously in coarse-grained electrodeposition applications [43, 44]. The details of the simulation code algorithm are also described briefly in the Appendix, and in detail elsewhere. A $(2+1)$D solid-on-solid KMC algorithm was constructed for simulating deposit growth and surface roughness analysis by following approaches reported previously [39]. By this approach, the lattice sites consist only of 2D "interface" sites on the surface for which the "roughness" is accounted for in the "$+1$D" component.

All simulations presented in this work were run on a Dell Xeon Linux cluster (National Center for Supercomputing Applications, NCSA), on a 3.06 GHz Intel Xeon processor. The simulation time depended on the physicochemical parameters used in the simulations and was a strong function of the surface diffusion energy barriers. For each set of conditions for which results are reported below, twenty simulations were carried out with different seed numbers for the random number generator and the simulation results were averaged.

The KMC simulations produced a variety of outputs, including snapshots of the surface morphology and statistical data. As described elsewhere [39], a simulation data post-processor computed the cluster density, size distribution, etc. For the purposes of analysis, a cluster was defined as a group of two or more adjacent metal atoms.

3. Results and discussion

The results reported here consider deposition onto a substrate seeded with various numbers and spacings of 10-atom metal clusters. The physicochemical parameters used in the simulations are listed in Table 1 are the same as used previously [39]. The metal–substrate energy barrier for surface diffusion (E_{M-S}) was varied between 2.5×10^{-20} and 5.5×10^{-20} J, a range that has been shown to exhibit a large change in surface morphology. All snapshots of the surface shown in the figures below are for one of the twenty seed numbers which were run for a particular parameter set in the KMC simulation code.

Table 1. Input physicochemical parameters used in the KMC simulations.

Parameter	Value
Deposition rate constant for M on M, k_{M-M}	$0.204\,m^3/mol\,s^{-1}$
Equilibrium potential for M deposition on M	0 V
Charge transfer coefficient for M deposition on M, α_{M-M}	0.5
Deposition rate constant for M on S, k_{M-S}	$2.04\,m^3/mol\,s^{-1}$
Nucleation overpotential for M deposition on S	−0.10 V
Charge transfer coefficient for M deposition on S, α_{M-S}	0.5
Jump frequency for M surface diffusion on M, w_{M-M}	$1.50 \times 10^{16}\,s^{-1}$
Energy barrier for breaking a M–M bond, E_{M-M}	4×10^{-20} J
Jump frequency for M surface diffusion on S, w_{M-S}	$1.50 \times 10^{16}\,s^{-1}$
Energy barrier for breaking a M–S bond, E_{M-S}	2.5×10^{-20} to 5.5×10^{-20} J
Temperature, T	298 K
Applied potential	−0.11, −0.12, −0.13 V
M^{2+} concentration at surface	0.1 M

3.1 Substrates seeded with 49 metal clusters

A square array of 49 seed clusters spaced 11 nm apart was investigated, a physical arrangement that corresponds to configurations produced experimentally by Kolb *et al.* [21]. Simulations were performed until such time that 0.25 equivalent monolayers (ML) of metal were deposited; snapshots of the surface were recorded after each 0.05 ML of metal was deposited. Simulations were performed for three different applied potentials (−0.11, −0.12, and −0.13 V).

Electrodeposition may occur on the seed clusters (M) as well as on the substrate (S). Simulation results reported in Fig. 2, for the case of deposition at −0.11 V, illustrate that the number of secondary nuclei (*i.e.*, nuclei not connected to a seed clusters) depend on E_{M-S} (the metal–substrate surface diffusion energy barrier), and time (expressed as fractions of monolayers deposited). For each data point in Fig. 2, the error bars computed with 20 seed numbers were no greater than the size of the symbol used to represent the data point; in most cases the error bars were less than 4% which corresponds to the width of the solid line used to connect the data points. For the case of 0.05 ML, the number of secondary nuclei is negligible for $E_{M-S} = 2.5 \times 10^{-20}$ J and increases with E_{M-S} through a maximum at 4.0×10^{-20} J. The observation that the number of secondary nuclei is the lowest for low values of E_{M-S}, is consistent with the interpretation that metal atoms deposited on the substrate would readily move by surface diffusion to low energy sites provided by an existing seed cluster on the surface. It is also seen in Fig. 2 that for E_{M-S} above 4.0×10^{-20} J, and depending on the value of monolayer coverage, the number of secondary nuclei decreases. The reason that the number of secondary nuclei decreases for values of E_{M-S} higher than 4.0×10^{-20} J is that under these conditions there

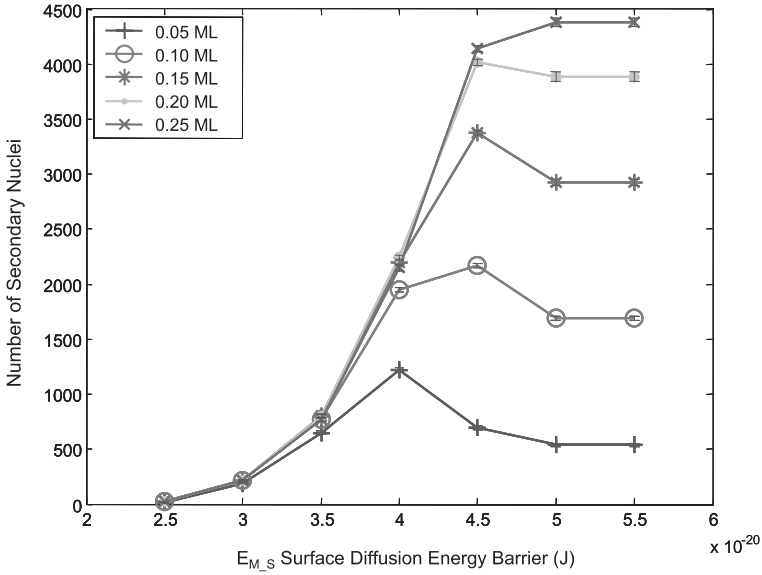

Fig. 2. Number of secondary nuclei as a function of the metal–substrate surface diffusion energy barrier and time for deposition at −0.11 V.

are many single atoms on the surface (which are not counted as "two-atom clusters"), and the deposited atoms cannot readily move about by surface diffusion on the substrate. As time progresses in the simulations, these single atoms become secondary nuclei when subsequent deposition results in new adatoms being located in adjacent lattice sites. Thus, for example at 0.25 ML of metal deposition, the largest number secondary nuclei is seen for the highest values of E_{M-S}. Moreover, it may be seen that the curves in Fig. 2 converge onto a common curve along the left-hand side. That is, for a given value of E_{M-S}, there is an upper limit to the number of secondary nuclei that are formed, and that limiting value is reached sooner for lower values of $E_{M-S.}$

For the parameter values used for the results shown in Fig. 3, it may be seen that the average cluster size increases with extent of deposition (fraction of monolayers deposited) for low values of E_{M-S}, whereas for high values of E_{M-S}, the average cluster size remained constant as a function of time. Consider a fabrication process where 49 seed clusters placed on a surface are to be grown under conditions that minimize the formation of secondary nuclei. For the range of parameters investigated here, the simulation results in Figs. 2 and 3 indicate that the substrate material should be selected so that $E_{M-S} < 3.5 \times 10^{-20}$ J, in order to produce a uniform size distribution of the seed clusters.

For the case of 0.25 ML and with the parameters listed in Table 1, additional sets of simulation results are reported in Figs. 4 and 5 for various applied potentials. In addition, Fig. 4 shows snapshots of the cluster morphology for

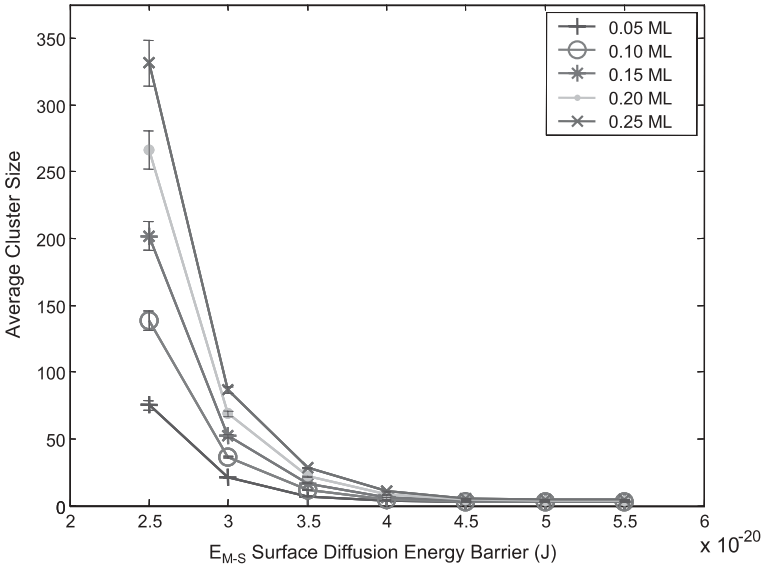

Fig. 3. Average cluster size as a function of the metal–substrate surface diffusion energy barrier and time for deposition at −0.11 V.

various values of $E_{M\text{–}S}$ and applied potential. As seen in the graph in Fig. 4, a small increase in applied potential results in a small increase in the number of secondary nuclei. However, there does not appear to be a significant change in morphology over the small range of applied potential associated with the three snapshots in Fig. 4a–c (low $E_{M\text{–}S}$), nor for the three snapshots in Fig. 4d–f (high $E_{M\text{–}S}$). The data in Fig. 5 illustrate that, for low values of $E_{M\text{–}S}$, the average cluster size was smaller for simulations performed at higher applied potentials. Furthermore, Fig. 5 indicates that for large values of $E_{M\text{–}S}$ ($> 3.5 \times 10^{-20}$ J), the average cluster size does not change appreciably as a function of the applied potential. Collectively, these results imply that, in order to fabricate an array of metal deposits by growing seed clusters under kinetically limited conditions, the deposition should be performed at a low applied potential because the average cluster size is larger and the number of secondary nuclei formed is lower.

For the case of 0.25 ML of deposit, with $E_{M\text{–}S} = 2.5 \times 10^{-20}$ J, Fig. 6a, c and e illustrate the dependence of cumulative cluster size distribution on the number of atoms in the cluster for three values of applied potential. For these results, simulation results from 20 independent seed number simulations were used to construct the cumulative distributions and a cubic spline curve was fit to the cumulative distribution function produced from those data. It may be seen that there are two "bumps" in the normalized cumulative distribution function, which indicates that there is bimodal distribution of the cluster size in all of the

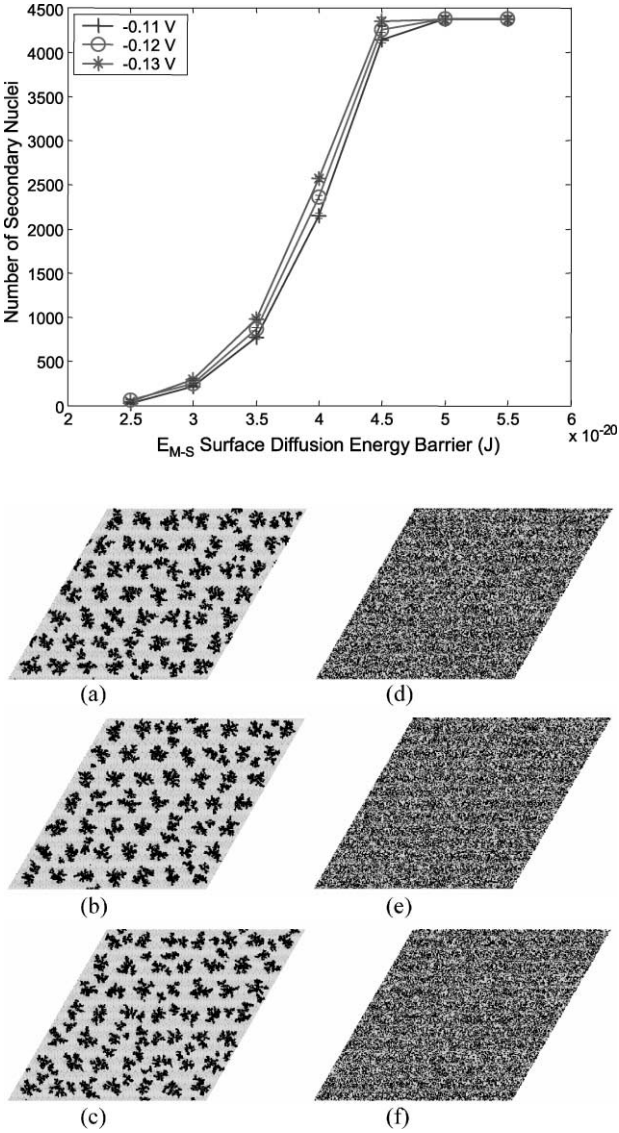

Fig. 4. Number of secondary nuclei after 0.25 ML metal has been deposited as a function of the metal–substrate surface diffusion energy barrier and applied potential. Snapshots of the surface are for
(a) $E_{M\text{–}S} = 2.5 \times 10^{-20}$ J and applied potential $= -0.11$ V,
(b) $E_{M\text{–}S} = 2.5 \times 10^{-20}$ J and applied potential $= -0.12$ V,
(c) $E_{M\text{–}S} = 2.5 \times 10^{-20}$ J and applied potential $= -0.13$ V,
(d) $E_{M\text{–}S} = 5.5 \times 10^{-20}$ J and applied potential $= -0.11$ V,
(e) $E_{M\text{–}S} = 5.5 \times 10^{-20}$ J and applied potential $= -0.12$ V, and
(f) $E_{M\text{–}S} = 5.5 \times 10^{-20}$ J and applied potential $= -0.13$ V.

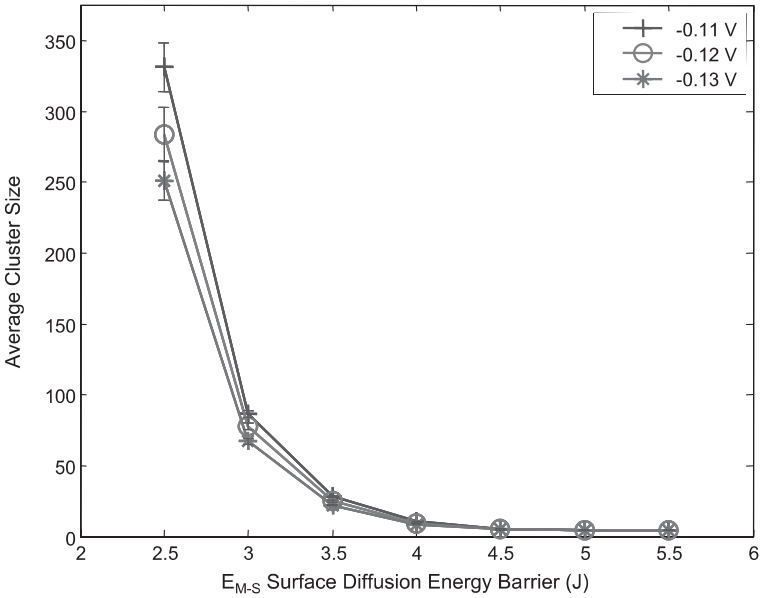

Fig. 5. Average cluster size after 0.25 ML of metal has been deposited as a function of the metal–substrate surface diffusion energy barrier and applied potential.

simulations. Figure 6b, d, and f illustrates results for cluster size distributions obtained by taking the derivative of the cubic spline fit to the cumulative distribution, followed by application of a second-order acausal filter [45] with a filter constant of 0.1 to smooth the sharp jumps at the knots of the cubic spline function. In the bimodal distributions observed in Fig. 6b, d, and f, the first peak (located at a lower number of atoms) is due to secondary nuclei, while the second peak corresponds to the growth of the seed clusters originally present on the substrate. As the applied potential is increased (made more negative), the first peak becomes higher relative to the second peak and the second peak shifts to the left and becomes centered at a point where there is a lower number of atoms in a cluster. The results in Figs. 5 and 6 indicate that at a lower applied potential, it is possible to obtain larger clusters with a smaller number of secondary nuclei formed. From the point of view of controlling the cluster size distribution, it is worth noting that a small shift in the applied potential (0.01 V) has a relatively large influence on relative number of secondary nuclei formed during growth of the seed nuclei.

3.2 Effect of seed cluster density

In the following set of simulations, the number of clusters placed on the surface was varied to determine the effect that the number of seed clusters has on the

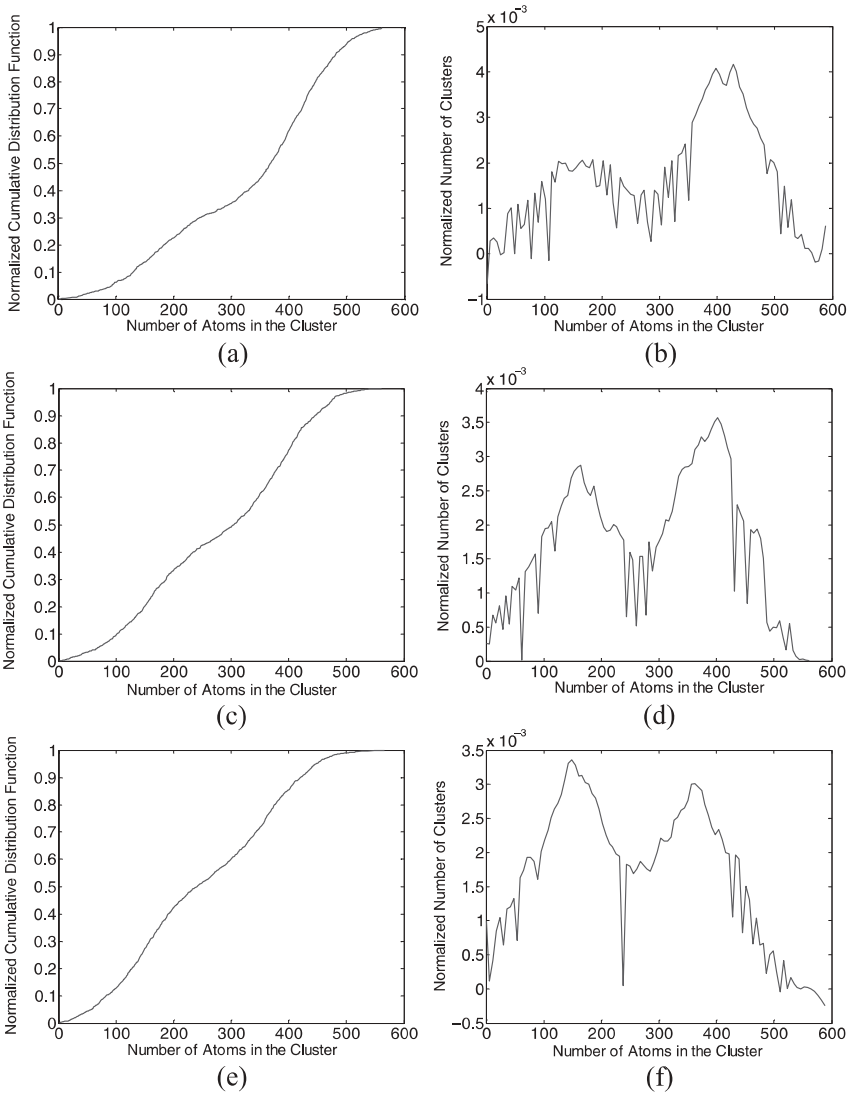

Fig. 6. Normalized cumulative distribution function and normalized number of clusters as a function of the number of atoms in the cluster after 0.25 ML of metal have been deposited and $E_{M-S} = 2.5 \times 10^{-20}$ J for applied potential of a,b) -0.11 V, c,d) -0.12 V, and e,f) -0.13 V.

number of secondary nuclei formed and the cluster size distribution. The simulations were performed until 0.25 equivalent monolayers (ML) of metal were deposited (not including the seed cluster material) and snapshots of the surface

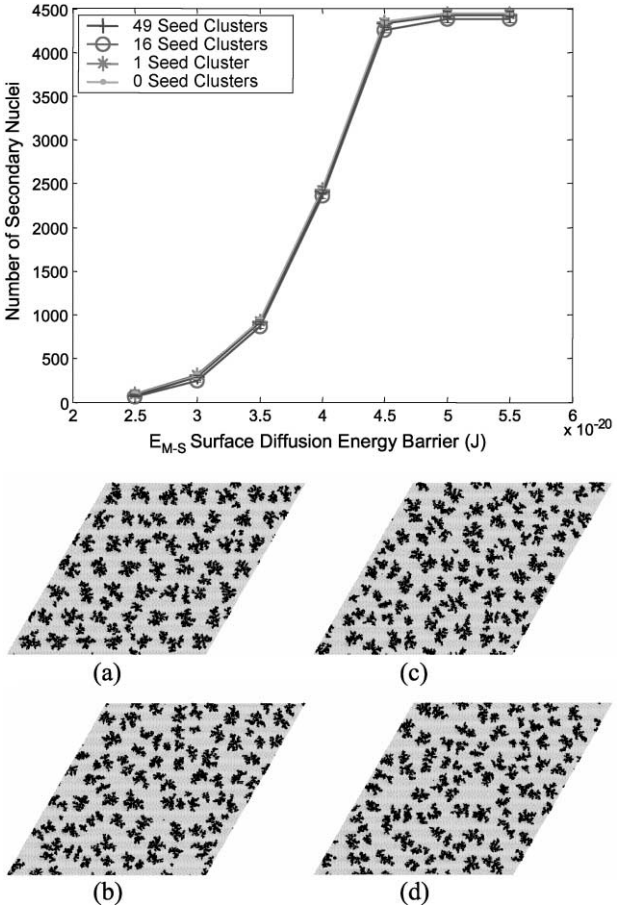

Fig. 7. Number of secondary nuclei after 0.25 ML metal has been deposited as a function of the metal–substrate surface diffusion energy barrier and number of metal seed clusters. Snapshots of the surface are for
(a) $E_{M\text{–}S} = 2.5 \times 10^{-20}$ J and 49 metal seed clusters,
(b) $E_{M\text{–}S} = 2.5 \times 10^{-20}$ J and 16 metal seed clusters,
(c) $E_{M\text{–}S} = 2.5 \times 10^{-20}$ J and 1 metal seed clusters, and
(d) $E_{M\text{–}S} = 2.5 \times 10^{-20}$ J and 0 metal seed clusters.

were recorded after each 0.05 ML of metal was deposited. Simulations were performed for three different seed configurations: (1) 16 seed clusters evenly spaced in a square pattern on the surface, 19.2 nm apart; (2) one seed cluster in the middle of the simulation domain; and (3) no seed clusters In all cases, deposition was performed at -0.12 V.

In Fig. 7, the number of secondary nuclei is shown as function of $E_{M\text{–}S}$ and the number of seed clusters. For all values of $E_{M\text{–}S}$ investigated here, the num-

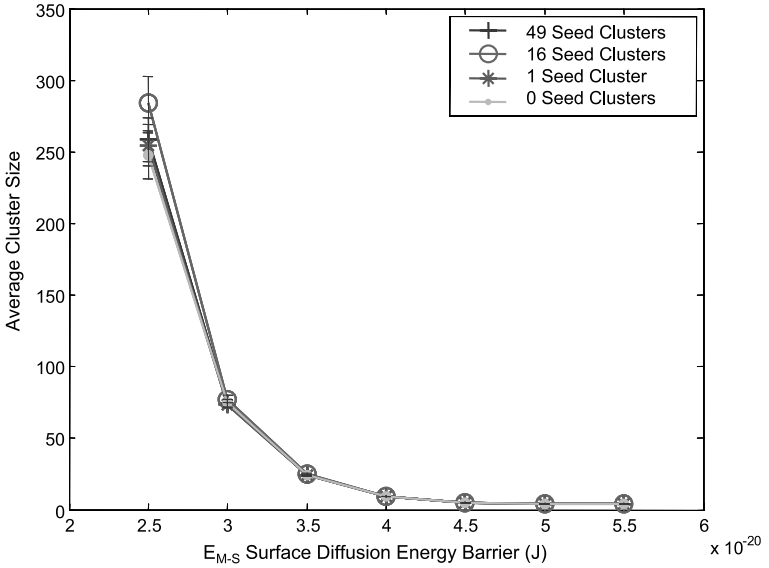

Fig. 8. Average cluster size after 0.25 ML metal has been deposited as a function of the metal–substrate surface diffusion energy barrier and number of metal seed clusters.

ber of secondary nuclei formed does not depend on the number of seed clusters. Figure 7a–d show that the morphology of the clusters grown with different numbers of seed clusters is similar, although the pattern in Fig. 7a (with 49 seed clusters) may be recognized as being more ordered on the surface.

The average cluster size is shown as a function of E_{M-S} in Fig. 8 for the variously seeded surfaces. For all values of E_{M-S} except 2.5×10^{-20} J, the average cluster size is only weakly dependent on the number of seed clusters. For the conditions investigated here, these results indicate that there is a clear advantage seeding a surface to grow a certain cluster distribution only for $E_{M-S} < 3.5 \times 10^{-20}$ J In the simulations where $E_{M-S} = 2.5 \times 10^{-20}$ J, the smallest average cluster size was obtained for the substrate with no seed clusters, since *all* nuclei formed on the surface are equivalent to the "secondary nuclei." For the parameter values used here, the largest average cluster size was obtained in the simulations with 16 seed clusters. The issue of predicting optimum conditions for growth of seed clusters in the absence of secondary nuclei, and in the presence of solution additives, is under continued study in our laboratory and will be reported in subsequent publications.

The effect of seed cluster density on cumulative distribution functions is shown in Fig. 9a, c, e, and g after 0.25 ML of metal has been deposited, for $E_{M-S} = 2.5 \times 10^{-20}$ J. The cluster distributions in Fig. 9b, d, f, and h were computed as described previously. It may be seen that the cumulative distribution function is clearly bimodal only for the case of 49 seed clusters, seen in Fig. 9a

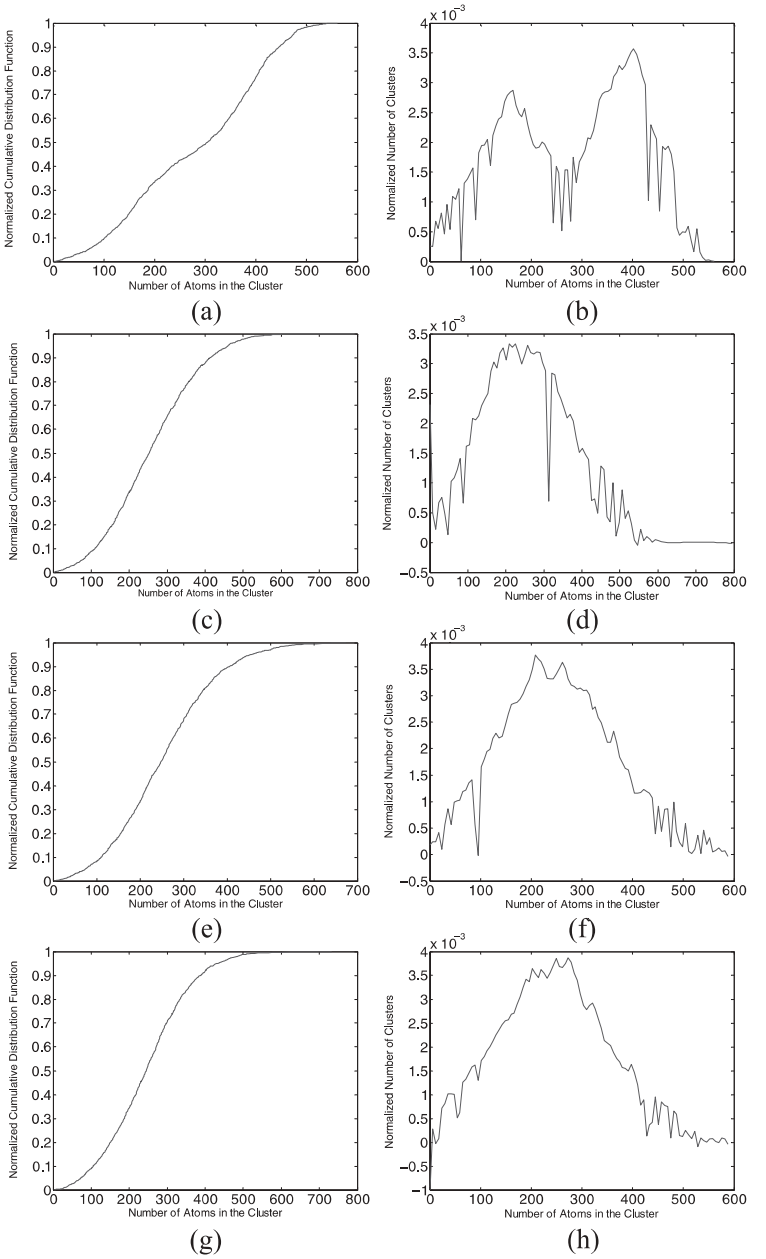

Fig. 9. Normalized cumulative distribution function and normalized number of clusters as a function of the number of atoms in the cluster after 0.25 ML of metal have been deposited and $E_{M-S} = 2.5 \times 10^{-20}$ J for surfaces with a,b) 49, c,d) 16, e,f) 1, and g,h) 0 metal seed clusters.

and b. For the cases with 0, 1, and 16 seed clusters only one peak is observed in the cluster distributions (see Fig. 9d, f, and h), and that peak is dominated by secondary nuclei. As the number of seed clusters on the surface was reduced, the width of the peak that is attributed to the secondary nuclei that have formed during deposition becomes wider, which indicates that the cluster distribution was less uniform when there were fewer seed clusters on the surface. Although the average cluster size was similar for all of the seeded surfaces when $E_{M-S} = 2.5 \times 10^{-20}$ J (see Fig. 8), Fig. 9b, d, f and h. show that the distribution of the cluster size was very different based on the number of seed clusters on the surface. When more clusters were seeded on the surface it was possible to grow larger clusters with a more uniform size distribution (as shown in Fig. 9c and d).

4. Conclusions

A kinetic Monte Carlo simulation model was developed to investigate the growth of seed clusters of metal (M) on a substrate (S) by electrodeposition. Numerical results were obtained on the effect of the number of seed clusters, the applied potential, and the metal–substrate surface diffusion energy barrier. It was found that the best conditions for producing a uniform cluster size distribution were to have a high number of seed clusters initially on the surface, to have a low applied potential, and to have a low metal–substrate surface diffusion energy barrier.

It was found that with low values of E_{M-S}, the average cluster size continually increased with time and for high values of E_{M-S}, the average cluster size remained constant as a function of time. Given the parameters used in the simulations, these results suggest that a substrate material should be selected so that $E_{M-S} < 3.5 \times 10^{-20}$ J to obtain a uniform size distribution of the clusters. For large values of E_{M-S} ($> 3.5 \times 10^{-20}$ J), the average cluster size does not change as a function of the applied potential. These results imply that the deposition should be performed at a low applied potential with a substrate that has a low value of E_{M-S}, to produce a uniform cluster size distribution under kinetically limited conditions.

For the M–S system studied here and for all values of E_{M-S} except 2.5×10^{-20} J, the average cluster size was found to be weakly dependent on the number of seed clusters. The results indicate that there is no clear advantage to seeding a surface where $E_{M-S} \geq 3.5 \times 10^{-20}$ J to obtain a desired cluster distribution, for the parameter set and conditions simulated. In the simulations where $E_{M-S} = 2.5 \times 10^{-20}$ J, the smallest average cluster size was obtained for the substrate with no seed clusters.

The cumulative distribution functions showed that when more clusters are seeded on the surface it was possible to grow larger clusters with a uniform size distribution, up to a certain limit at which point further increases in the num-

ber of clusters resulted in a bimodal distribution. At a lower applied potential, it was possible to obtain larger clusters with a smaller number of secondary nuclei formed.

Acknowledgement

The authors acknowledge with appreciation helpful discussions with Ryan Stephens at the University of Illinois. Funding for this work was provided by an IBM Faculty Partnership and the National Science Foundation under grants ACI 96-19019, CTS-0135621 and -0438356, and NSF PACI NRAC MCA-01S022. Any opinions, findings, and conclusions or recommendations expressed in this material are those of the authors and do not necessarily reflect the views of the National Science Foundation. The first author received funding from the H. G. Drickamer Fellowship from the Department of Chemical and Biomolecular Engineering at the University of Illinois.

Appendix

The guiding principles for code development were to focus on interactions between the deposited metal (M) and substrate (S) for several limiting cases of behavior involving relative rates of electrodeposition rate and surface diffusion. The geometric details of the substrate and metal deposit were kept purposely simple, as was the reaction chemistry. (although the code was written to accept more complicated substrate configurations as well as mechanisms involving additional reactions and intermediate species associated with electrodeposition additives).

In the system there are N species that can possibly undergo k transition events [46], which each have an associated rate, R_i. The N species are partitioned over the possible transition events. Once the rates of the events are calculated, a list of transition probabilities can be constructed in terms of the rates in such a way that there is a dynamical hierarchy established between the rates. The individual transition probabilities are

$$W_i = \frac{r_i}{\xi_{\max}}, \tag{A-1}$$

where $\xi_{max} \geq \sum_i r_i$. A sufficiently large system is used to maintain the independence of the events, which is verified by computing the autocorrelation function of output parameters of the simulations.

The KMC algorithm is similar to those described by Levi and Kotrla [47] and Battaile *et al.* [48]:

1. Choose a random number, r, from a uniform distribution in the range (0,1).
2. Select the transition event from the list by selecting the first index s for which $\sum_{j=1}^{s} r_j \geq r$.

3. Proceed with r_j.
4. Update all r_j that have changed as a result of making the move.
5. Advance the time in the simulations by τ_i, where

$$\tau_i = \frac{1}{\sum_i n_i r_i} \tag{A-2}$$

and n_i is the number of species out of N that are capable of undergoing a transition event with rate r_i [49, 50].

This algorithm decreases the simulation time by binning the rates by type. Each time a rate is selected, an instance of that rate is executed. The instance of the rate is selected based on the same random number generated to select which rate is executed.

The KMC algorithm can be implemented in several different ways. The goal is to implement the algorithm in the most computationally efficient manner so that large discretizations of the simulation domain can be simulated. The following describes details on how the algorithm is coded, including the storage and search algorithms that are used.

1. Information about each rate is stored in a matrix. The site number is unique for each site on the surface. Periodic boundary conditions are used in the x and y directions.
2. At the beginning of the simulation, all of the rates for all possible moves are tabulated and cataloged. These rates are only recalculated when a move occurs at a site or one of its eight nearest neighbor sites.
3. All of the possible rates in the system are binned to create a list that is used to select what events occur.
4. The rates are normalized and a random number is generated on the interval (0,1).
5. Once the random number is generated, the appropriate event is selected from the list.
6. An instance of that event is selected from the bin for that rate and the action is executed.
7. The appropriate neighbor rates are updated in the site list depending on the action that is taken.
8. The time in the system is updated and the process is repeated from steps 3–8 until the user-specified deposition time has been reached.

List of symbols

$E_{\mathrm{M–M}}$ surface diffusion energy barrier for breaking an M–M bond, J
$E_{\mathrm{M–S}}$ surface diffusion energy barrier for breaking an M–S bond, J
$k_{\mathrm{M–M}}$ rate constant for deposition of species M^{2+} on surface M, $\mathrm{m^3/mol\,s^{-1}}$

k_{M-S} rate constant for the deposition of species M^{2+} on surface S, $m^3/mol\,s^{-1}$
n_i number of particles out of N that are capable of undergoing a transition event with rate r_i
r_i rate of transition event i
T temperature, K
w_{M-S} jump frequency for surface diffusion of species M on surface S, s^{-1}
w_{M-M} jump frequency for surface diffusion of species M on surface M, s^{-1}
W_i probability of transition event i occurring, Eq. (A-1), dimensionless

Greek symbols

α_{M-S} charge transfer coefficient for the deposition of species M^{2+} on surface S, dimensionless
α_{M-M} charge transfer coefficient for the deposition of species M^{2+} on surface M, dimensionless
ξ_{max} scaling parameter which, when selected sufficiently large, ensures that the transition probabilities are small enough to simulate correctly the dynamics, s^{-1}
$\Delta\tau$ time step in kinetic Monte Carlo algorithm, Eq. (A-2), s

References

1. R. Alkire, J. Electroanal. Chem. **559** (2003) 3.
2. R. Alkire and R. Braatz, AIChE Journal **50** (2004) 2000.
3. D. M. Kolb, *The Initial Stages of Metal Deposition as Viewed by Scanning Tunneling Microscopy.* In *Adv. Electrochem. Science and Engr.* R. Alkire and D. Kolb (Eds.), Vol. 7, Wiley-VCH, Weinheim, Germany (2002), pp. 107–150.
4. W. J. Lorenz and W. Plieth (Eds.), *Electrochemical Nanotechnology: In-situ Local Probe Techniques at Electrochemical Interfaces*. Wiley-VCH, Weinheim, Germany (1998).
5. P. L. Hansen, J. B. Wagner, S. Helveg, J. R. Rostrup-Nielsen, B. S. Clausen, and H. Topsøe, Science **295** (2002) 2053.
6. A. S. Claye, J. E. Fischer, C. B. Huffman, A. G. Rinzler, and R. E. Smalley, J. Electrochem. Soc. **147** (2000) 2845.
7. J. L. Stickney, *Electrochemical Atomic Layer Epitaxy: Nanoscale Control in the Electrodeposition of Compound Semiconductors.* In *Adv. Electrochem. Sci. and Engr.* R. Alkire and D. Kolb (Eds.), Vol. 7, Wiley-VCH, Weinheim, Germany (2002), pp. 1–106.
8. G. Fasol and K. Runge, Appl. Phys. Lett. **70** (1997) 2467.
9. G. Fasol, Science **280** (1998) 545.
10. R. Liu, E. W. Bohannan, H. M. Kothari, and J. A. Switzer, Appl. Phys. Lett. **83** (2003) 1944.
11. J. A. Switzer, *Electrodeposition of Superlattices and Multilayers.* In: *The Electrochemistry of Nanostructures: Preparation and Properties*. G. Hodes (Ed.), Wiley-VCH, Weinheim, Germany (2001), pp. 67–101.
12. H. M. Kothari, A. A. Vertegel, E. W. Bohannan, and J. A. Switzer, Chem. Mater. **14** (2002) 2750.

13. A. H. Ali and C. A. Foss, Jr., J. Electrochem. Soc. **146** (1999) 628.
14. X. Dang, A. M. Massari, and J. T. Hupp, Electrochem. Solid State Lett. **3** (2000) 555.
15. J. J. Kelly, P. E. Bradley, and D. Landolt, J. Electrochem. Soc. **147** (2000) 2975.
16. L. Cheng and S. Dong, J. Electrochem. Soc. **147** (2000) 606.
17. W. Schindler, D. Hofmann, and J. Kirschner, J. Electrochem. Soc. **148** (2001) C124.
18. M. S. Sandler and L. Tan, Adv. Func. Mat. **13** (2003) 393.
19. D. M. Kolb, R. Ullmann, and T. Will, Science, **275** (1997) 1097.
20. D. M. Kolb, R. Ullmann, and J. C. Ziegler, Electrochim. Acta, **43** (1998) 2751.
21. G. E. Engelmann, J. C. Ziegler, and D. M. Kolb, Surf. Sci. **401** (1998) L420.
22. J. C. Ziegler, G. E. Engelmann, and D. M. Kolb, Z. Phys. Chem. **208** (1999) 151.
23. R. T. Poetzschke, G. Staikov, W. J. Lorenz, and W. Wiesbeck, J. Electrochem. Soc. **146** (1999) 141.
24. J. T. Moore, P. D. Beale, T. A. Winningham, and K. Douglas, Appl. Phys. Lett. **72** (1998) 1840.
25. J. Carrey, J.-L. Maurice, P. Jensen, and A. Vaurès, Appl. Surf. Sci. **164** (2000) 48.
26. H. Liu, F. Favier, K. Ng, M. P. Zach, and R. M. Penner, Electrochim. Acta **47** (2001) 671.
27. D. J. Riley, Cur. Opin. In Col. & Surf. Sci. **7** (2002) 186.
28. G. Schmid, Adv. Eng. Mat. **3** (2001) 737.
29. F. Remacle and R. D. Levine, Appl. Phys. Lett. **82** (2003) 4543.
30. R. Pool, Science, **248** (1990) 1186.
31. S. Rohart, G. Baudot, V. Repain, Y. Girard, S. Rousset, H. Bulou, C. Goyhenex, and L. Proville, Surf. Sci. **559** (2004) 47.
32. G. Brown, P. A. Rikvold, M. A. Novotny, and A. Wieckowski, J. Electrochem. Soc. **146** (1999) 1035.
33. M. F. Gyure, Comp. in Sci. and Eng. **1** (1999) 100.
34. M. C. Bartelt and J. W. Evans, Phys. Rev. B **46** (1992) 12 675.
35. L. Nurminen, A. Kuronen, and K. Kaski, Phys. Rev. B **63** (2000) 035407-1.
36. F. Elsholz, M. Meixner, and E. Schöll, Nuc. Inst. Meth. in Phys. Res. B **202** (2003) 249.
37. M. G. Del Pópolo, E. P. M. Leiva, M. Mariscal, and W. Schmickler, Nanotech. **14** (2003) 1009.
38. M. C. Giménez, M. G. Del Pópolo, E. P. M. Leiva, S. G. Garcia, D. R. Salinas, C. E. Mayer, and W. J. Lorenz, J. Electrochem. Soc. **149** (2002) E109.
39. T. O. Drews, A. Radisic, J. Erlebacher, R. D. Braatz, P. C. Searson, and R. C. Alkire, J. Electrochem. Soc. **153** (2006) C434.
40. R. M. Stephens and R. C. Alkire, J. Electrochem. Soc. **154** (2007) D418.
41. T. O. Drews, *PhD Thesis*. University of Illinois at Urbana-Champaign (2004).
42. A. Radisic, *PhD Thesis*. Johns Hopkins University (2004).
43. T. O. Drews, R. D. Braatz, and R. C. Alkire, Int. J. Multiscale Comp. Eng. **2** (2004) 313.
44. X. Li, T. O. Drews, E. Rusli, F. Xue, Y. He, R. Braatz, and R. Alkire, J. Electrochem. Soc. **154** (2007) D230.
45. W. H. Press, B. P. Flannery, S. A. Teukolsky, and W. T. Vetterling, *Numerical Recipes in C: The Art of Scientific Computing*. Cambridge University Press, 2nd ed. (1992) p. 559.
46. K. A. Fichthorn and W. H. Weinberg, J. Chem. Phys. **95** (1991) 1090.
47. A. C. Levi and M. Kotrla, J. Phys. Condens. Matter **9** (1994) 299.
48. C. C. Battaile, D. J. Srolovitz, and J. E. Butler, J. Appl. Phys. **82** (1997) 6293.
49. Y. G. Yang, R. A. Johnson, and H. N. G. Wadley, Surf. Sci. **499** (2002) 141.
50. G. Henkelman and H. Jónsson, J. Chem. Phys. **115** (2001) 9657.